Bioorganic & Medicinal Chemistry xxx (xxxx) xxx–xxx

Contents lists available at ScienceDirect

Bioorganic & Medicinal Chemistry

journal homepage: www.elsevier.com/locate/bmc

Design, synthesis and anticancer evaluation of acridine hydroxamic acid derivatives as dual Topo and HDAC inhibitors

Jiwei Chen[a,b,f], Dan Li[a,b,f], Wenlu Li[a,b], Jingxian Yin[a,b], Yueying Zhang[a,b], Zigao Yuan[b,e,*], Chunmei Gao[d], Feng Liu[a,b,*], Yuyang Jiang[b,c]

[a] Department of Chemistry, Tsinghua University, Beijing 100084, PR China
[b] State Key Laboratory of Chemical Oncogenomics, Key Laboratory of Chemical Biology, The Graduate School at Shenzhen, Tsinghua University, Shenzhen, Guangdong 518055, PR China
[c] Department of Pharmacology and Pharmaceutical Sciences, School of Medicine, Tsinghua University, Beijing 100084, PR China
[d] College of Chemistry and Chemical Engineering, Shenzhen University, Shenzhen 518060, PR China
[e] Shenzhen Kivita Innovative Drug Discovery Institute, Shenzhen 518055, PR China

ARTICLE INFO

Keywords:
Topoisomerase
Histone deacetylase
Dual inhibitor
Drug design
Anticancer

ABSTRACT

Multitarget inhibitors design has generated great interest in cancer treatment. Based on the synergistic effects of topoisomerase and histone deacetylase inhibitors, we designed and synthesized a new series of acridine hydroxamic acid derivatives as potential novel dual Topo and HDAC inhibitors. MTT assays indicated that all the hybrid compounds displayed good antiproliferative activities with IC_{50} values in low micromolar range, among which compound **8c** displayed potent activity against U937 (IC_{50} = 0.90 μM). In addition, compound **8c** also displayed the best HDAC inhibitory activity, which was several times more potent than HDAC inhibitor SAHA. Subsequent studies indicated that all the compounds displayed Topo II inhibition activity at 50 μM. Moreover, compound **8c** could interact with DNA and induce U937 apoptosis. This study provides a suite of compounds for further exploration of dual Topo and HDAC inhibitors, and compound **8c** can be a new dual Topo and HDAC inhibitory anticancer agent.

1. Introduction

Despite the exploitation of many new cancer treatments, such as gene and immunotherapy, chemotherapy is still the most effective strategy in clinical practice for most cancer patients. However, single-target chemotherapy strategies are often hindered by limited efficacy, toxic side effects and resistance. To solve these problems, multitarget ligand design has been a recent surge of research. Previous studies have revealed that multitarget ligands can modulate different targets simultaneously for cancer treatment and possess a greater therapeutic advantage than single-target drugs.[1,2]

The histone deacetylase (HDAC) is an attractive epigenetic target for cancer therapy. HDAC, together with histone acetyltransferase (HAT), determines the acetylation state of histone proteins. Overexpression of HDAC catalyzes deacetylation of lysine in histones, leading to chromatin condensation and tumor suppressor genes (TSGs) silencing in tumorigenesis.[3] HDAC inhibitors (HDACi) have been identified to reverse this process by binding HDAC, which can induce the expression of TSGs. To date, five HDAC inhibitors (i.e., Vorinostat, Depsipeptide, Belinostat, Panobinostat, and Chidamide) have come into the market. Most of them possess a well-admitted pharmacophore model composed of three groups: a zinc binding group (ZBG), a cap group, and a linker (Fig. 1).[4] HDACi have been demonstrated to successfully synergize with other targeted antitumor agents.[5–11]

Topoisomerases (Topo) are universal nuclear enzymes that modulate DNA supercoiling during DNA replication, transcription, and chromatin assembly by forming a reversible covalent Topo-DNA complex.[12,13] Topo I and Topo II are two types of DNA topoisomerases, which cleave single or double DNA strands, leading to transient DNA single-strand breaks or double-strand breaks, respectively. The mechanism of Topo inhibitors is to stabilize the DNA-enzyme cleavable complex through intercalation between DNA base pairs.[14] Acridine and acridone derivatives are one of the most potent inhibitors targeting Topo enzymes. Recently, many acridine analogues have been entered clinical or preclinical studies, such as *m*-AMSA, DACA, PZA, BRACO-19 and AS1410 (Fig. 2). Our group have also put efforts in synthesizing

* Corresponding authors at: State Key Laboratory of Chemical Oncogenomics, Key Laboratory of Chemical Biology, The Graduate School at Shenzhen, Tsinghua University, Shenzhen, Guangdong 518055, PR China.
E-mail addresses: yzg12@tsinghua.org.cn (Z. Yuan), liu.feng@sz.tsinghua.edu.cn (F. Liu).
[f] Jiwei Chen and Dan Li contributed equally.

https://doi.org/10.1016/j.bmc.2018.06.016
Received 28 March 2018; Received in revised form 12 June 2018; Accepted 13 June 2018

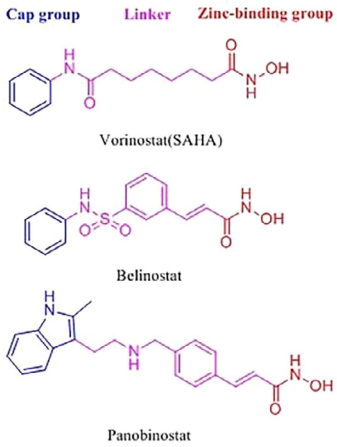

Fig. 1. Three approved HDAC inhibitors possessing a hydroxamic acid group.

several series of acridines with good antitumor activity.[15–20]

HDACi, which increase the accessibility of DNA by inducing DNA relaxation, can facilitate Topo inhibitors binding with chromatin and thus potentiate the antitumor sensitivity of Topo inhibitors.[21–23] Some Topo and HDAC inhibitors have been combined to treat cancer and displayed synergistic anticancer effects.[24–32] Besides, several hybrid compounds targeting both Topo and HDAC have been successfully synthesized with enhanced cytotoxicity.[33–40] These researches indicate that simultaneous inhibition of both Topo and HDAC could be a feasible approach on cancer therapy.

Considering the promising results, based on the structure of acridine drugs (Topo inhibitors, *m*-AMSA for example) and pharmacophore of HDACi (SAHA for example), a series of acridine hydroxamic acid derivatives were rationally designed and synthesized as potential dual Topo and HDAC inhibitors (Fig. 3).

2. Results and discussion

2.1. Chemistry

The synthetic routes of final compounds **8a–8f** and **12a–12b** were carried out as shown in Scheme 1. The acridine derivatives **1a–1b** were accomplished according to the reported procedures.[17,41] In the presence of phenol, compounds **3a–3d** were obtained by the reaction of commercially available ethynyl anilines **2a–2b** and **1a–1b**. Intermediates **6a–6b** were synthesized *via* NH_2OTHP and **5a–5b** produced by azide reaction of **4a–4b**. Compounds **3a–3d** reacted with **6a–6b** under nitrogen atmosphere giving compounds **7a–7f**. As shown in Scheme 1(a), target molecules **8a–8f** were produced by deprotection of **7a–7f**.

Amino acids **9** were heated with 9-chloroacridine derivatives **1a–1b** to give respective products **10a–10b**, which were then esterified to yield compounds **11a–11b** in methanol. The esters **11a–11b** were subjected to excessive amounts of hydroxylamine aqueous solution and sodium methylate to provide final products **12a–12b**, respectively (Scheme 1(b)).

2.2. In vitro enzymatic inhibitory assay

The inhibitory activities against HDAC1/6 and Topo I/II enzymes of the designed compounds were tested, and SAHA, camptothecin and *m*-AMSA were used as reference compounds.

The results (Table 1) apparently showed that all the compounds displayed outstanding inhibitory activities against HDAC1/6 with IC_{50} values in nanomolar ranges and that the activities against HDAC6 of almost all of the compounds were better than HDAC1. We were also pleased to find that **8a**, **8b**, **8c** and **8d** showed stronger inhibitory activities than HDAC inhibitor SAHA, among which compound **8c** displayed the best activity. After introducing the methoxy and chlorine groups to the acridine, the inhibitory activities against both HDAC1/6 resulted in a great reduction (**8a** *vs* **8e**, **8b** *vs* **8f**). When acridine was unsubstituted, the activities against HDAC6 of 5-carbon alkyl chain compounds were more potent than that of 6-carbon compounds (**8a** *vs* **8c**, **8b** *vs* **8d**). However, the activities against HDAC1 of 5-carbon alkyl chain compounds were less potent than 6-carbon compounds (**8a** *vs* **8c**, **8b** *vs* **8d**). Besides, the activities against both HDAC1/6 of *para*-position substitution on the benzyl ring compounds displayed better potencies than that of *meta*-position (**8a** *vs* **8b**, **8c** *vs* **8d**). As for substituted acridines, their inhibitory activities against HDAC6 were more potent than HDAC1, indicating that they may had selective tendencies on HDAC6 inhibition. In addition, **12a** possessed greatly decreased HDAC1/6 inhibitory activities in comparison with **8a** and **8c**, indicating that too short chain is not helpful for binding HDAC.

As we expected, our compounds could inhibit HDAC and Topo simultaneously. As shown in Fig. 4A, compound **12a** expressed strong Topo I inhibition potency at 100 μM which was more potent than the positive Topo I drug camptothecin. Excitingly, all the compounds displayed comparable Topo II inhibitory activities to the positive Topo II drug *m*-AMSA at 100 μM (Fig. 4B). Further research showed that all the compounds also presented good Top II inhibitory activity at 50 μM. These data suggest that all the compounds could potently inhibit Topo II. Furthermore, **12a** was dual Topo I/II inhibitors.

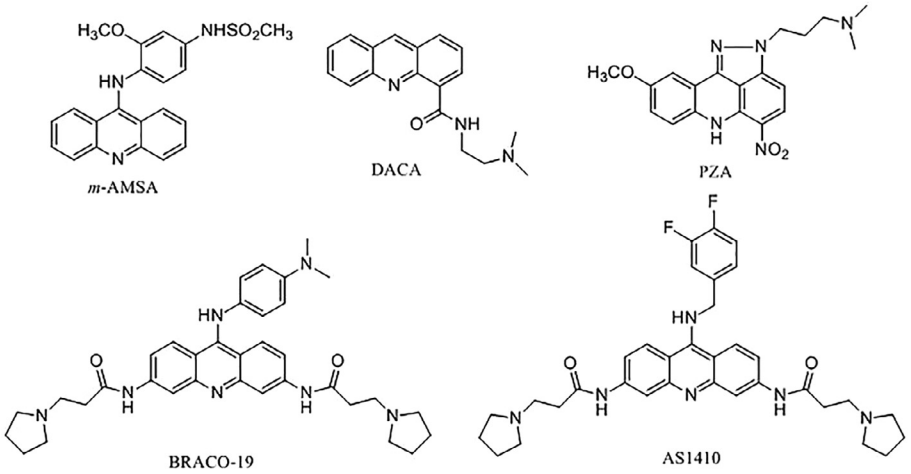

Fig. 2. The representative acridine derivatives in clinical or preclinical stages.

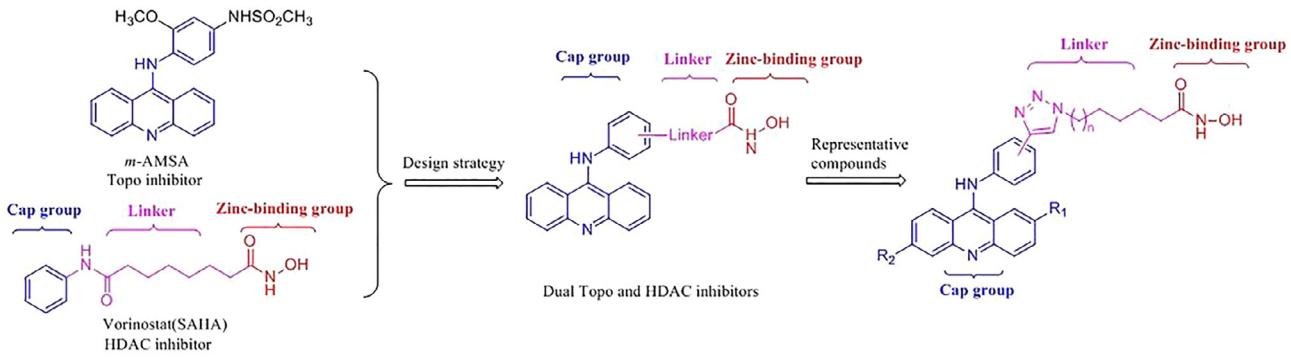

Fig. 3. Design of dual Topo and HDAC inhibitors.

2.3. Cell proliferation inhibitory assays

Lymphoma U937 cells were used in MTT assays to evaluate the antitumor activities of our synthesized compounds, with SAHA and *m*-AMSA used as the positive controls.

The results (Table 2) showed that all the final products displayed potent antiproliferative activity against U937 cells with IC_{50} values < 4 μM. Especially, compounds **8c** and **12a** displayed nanomolar IC_{50} values against U937, which were comparable with SAHA and *m*-AMSA. Compounds **8c** and **8d** exhibited more potent cytotoxic activities than **8a** and **8b** in U937, respectively. It can be obtained that when the acridine group was unsubstituted, the cytotoxic activities of 6-carbon alkyl chain compounds were generally better than that of 5-carbon compounds.

Furthermore, the antiproliferative activities were also related to the substitution pattern on the benzyl ring. When the acridine group was unsubstituted, **8a** and **8c** displayed better inhibitory activities than **8b** and **8d**, respectively, indicating that *para*-position is preferred than *meta*-position for cell proliferation inhibition. To our surprise, the introduction of methoxy and chlorine group led to obvious decrease of activities than the corresponding unsubstituted acridine derivatives (**8a** *vs* **8e**, **8b** *vs* **8f**, **12a** *vs* **12b**).[41]

As shown in Table 2, compound **8c** (IC_{50} = 0.90 μM) displayed improved antiproliferative activities against U937 than that of parent compound **7c** (IC_{50} = 21.39 μM). Similarly, compound **12a** also showed better cell proliferation inhibitory activities than **11a**, demonstrating that dual Topo and HDAC inhibitors **8c** and **12a** exhibited more potent antitumor potency than corresponding single target inhibitors of Topo.

As compounds **8c** and **12a** exhibited the best antiproliferative activity against U937 cells, they were chosen to test broad-spectrum antitumor activity. Results in Table 3 indicated that both **8c** and **12a** showed good antiproliferative activities against the human colon cancer cell line HCT-116. Compound **8c** also displayed more favorable inhibitory activities than Topo inhibitor *m*-AMSA against the human breast cancer cell line MDA-MB-231. The results also showed that they were more sensitive to U937.

2.4. DNA interaction studies

As compound **8c** displayed significant antiproliferative activity against cancer cell lines U937, MDA-MB-231, and HCT-116, it is necessary to study whether the interaction with DNA contributed to its cytotoxicity.

UV–visible spectral absorbance is a kind of widely used measure to detect the interaction between drugs and DNA. Fig. 5A displayed that the maximal absorption of compound **8c** was around 430 nm while DNA did not absorb light in this region. With the concentration of DNA increased, a significant decline in the absorption spectrum was observed. Besides, a slight bathochromic shift was shown, indicating that compound **8c** could intercalate into DNA.

The Formula (1) was used to calculate the DNA binding constant K_b, where DNA stands for the DNA concentration, meanwhile ε_a, ε_f represent the extinction coefficient of the complex free in solution, and ε_b is the extinction coefficient of the complex when fully bound to DNA respectively. As shown in Fig. 5B, the K_b of compound **8c** was $1.67 \times 10^5\,M^{-1}$, which suggested that it had a good DNA binding capability comparable to that of *m*-AMSA ($K_b = 1.36 \times 10^5\,M^{-1}$).

$$DNA/(\varepsilon_a-\varepsilon_f) = DNA/(\varepsilon_b-\varepsilon_f) + 1/K_b(\varepsilon_b-\varepsilon_f) \quad (1)$$

The fluorescence emission spectra was also performed to further study the DNA binding ability. Fig. 5C showed that compound **8c** had the emission peak at around 420 nm and 440 nm with an excitation wavelength at 360 nm. The fluorescence of **8c** was gradually quenched with increasing concentrations of DNA demonstrating the interaction between compound **8c** and DNA. The quenching constant K_q was calculated according to the classical Stern-Volmer Eq. (2). The quenching constant K_q of compound **8c** was $1.56 \times 10^5\,M^{-1}$, indicating that **8c** could intercalate into DNA.

$$F_0/\,F = 1 + K_qQ \quad (2)$$

2.5. Binding models of compound 8c with HDAC and Topo

To explore the binding models of compound **8c** with the respective enzymes, **8c** was docked into the active sites of HDAC2 (PDB code: 4LXZ), and Topo II-DNA complex (PDB code: 4G0U) using the SYBYL-X 1.3 protocol. Since the structure of HDAC2 (not HDAC1) crystallized with vorinostat has been solved, in this study, we chose HDAC2 which have identical active sites around the entrance of the channel with HDAC1 for molecular docking simulation study.[42]

As depicted in Fig. 6A, the 4-aminoacridine group occupies the surface outside the HDAC2 active pocket while the triazole-linked five carbons chain length extends to a proper distance thus leading the hydroxamic acid group to the active site and chelating with zinc. The hydroxamic acid group forms six hydrogen bonds with Tyr308, Asp181, His145, and His146. Fig. 6B suggests that the 9-amino acridine group was parallel to DG13 and forms a hydrogen bond with DNA. C-6 triazole-linked long alkyl chains of hydroxamic acid extends towards the hydrophilic region and forms four hydrogen bonds with Glu522, Ala521, and Arg503. The above docking results may further demonstrate the antiproliferative activity of **8c** was due to its inhibition against HDAC1/6 and Topo II.

2.6. Apoptosis induced by compound 8c

Compound **8c** could both inhibit the activity of HDAC 1/6 and Topo II. To further dissect the growth-inhibitory effects of our compounds, we evaluated the ability of **8c** to induce apoptosis in U937 cancer cells.

Apoptosis can be triggered by two key molecular signaling

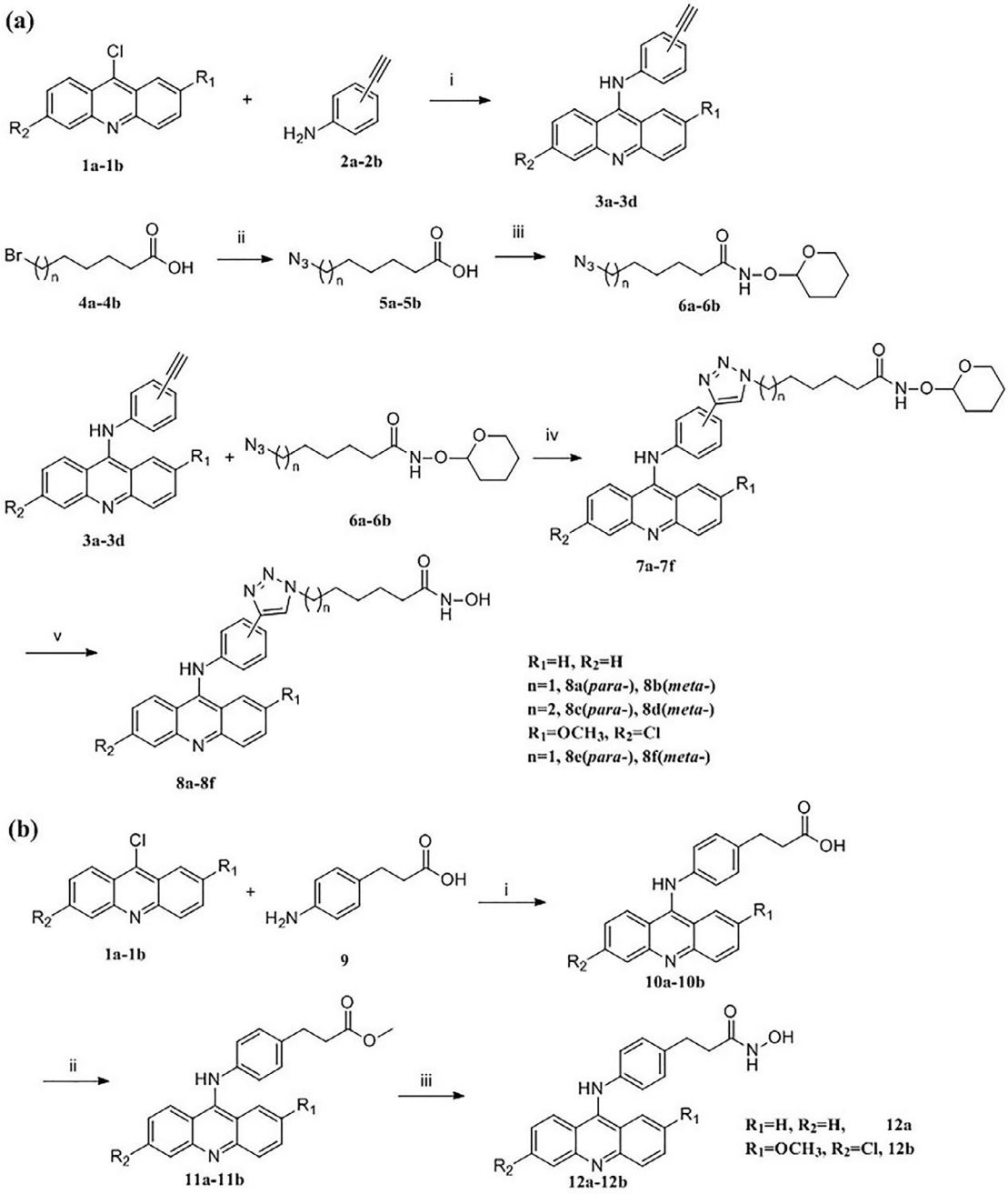

Scheme 1. Synthetic routes of final compounds **8a–8f** and **12a–12b**. Reagents and conditions: (a) (i) Phenol (solvent), 120 °C, 2 h; (ii) DMF, NaN_3, 80 °C, 2 days; (iii) EDCI, DMAP, $CHCl_3$, rt, NH_2OTHP; (iv) $CuSO_4{\cdot}5H_2O$, sodium ascorbate, H_2O: $C(CH_3)_3OH$ = 1: 1, 60 °C, 4 h; (v) CH_3OH, 3 M HCl, 2 h. (b) (i) Phenol (solvent), 120 °C, 2 h; (ii) $SOCl_2$, MeOH, 2 h; (iii) NH_2OH, CH_3ONa, CH_3OH: CH_2Cl_2 = 1: 1.

pathways: intrinsic pathway (mitochondrial pathway), extrinsic pathway (death-receptor-mediated pathway).[43] In order to validate which way that **8c** induced apoptosis, we monitored the expressions of regulatory proteins related to apoptotic pathway such as cleaved caspase-3, cleaved caspase-7, cleaved caspase-8 and cleaved caspase-9 in U937 cells by immunoblotting. Cleaved caspase-9 is involved in the intrinsic pathway, and cleaved caspase-8 is an initiator in extrinsic pathway. Activated caspase-9 and caspase-8 will further cleave downstream caspases including caspase-3 and caspase-7. As shown in Fig. 7, **8c** induced significant activation of cleaved caspase-9, caspase-8, caspase-3 and caspase-7 at 0 μM, 0.1 μM, 0.5 μM, 1 μM and 2.5 μM for 36 h, suggesting that both mitochondrial and death receptor pathways were involved in the **8c**-induced apoptosis.

3. Conclusion

In this study, a new series of acridine hydroxamic acid derivatives targeting both Topo and HDAC were designed and synthesized. All these compounds displayed potent antiproliferative activities against U937 cells *in vitro*. Among these compounds, compound **8c** showed not only nanomolar IC_{50} values against U937 but also the best HDAC1/6 inhibition activity, which was several times more potent than HDAC reference drug SAHA. What's more, **8c** displayed better Topo II inhibition activity at 50 μM and could interact with DNA and induce U937 apoptosis through both endogenous and exogenous pathway. Our studies suggested that compound **8c** targeting Topo and HDAC concurrently can be a new multitargeted inhibitory agent for cancer therapy.

Table 1
Enzymatic inhibitory activities of designed compounds against HDAC1 and HDAC6.

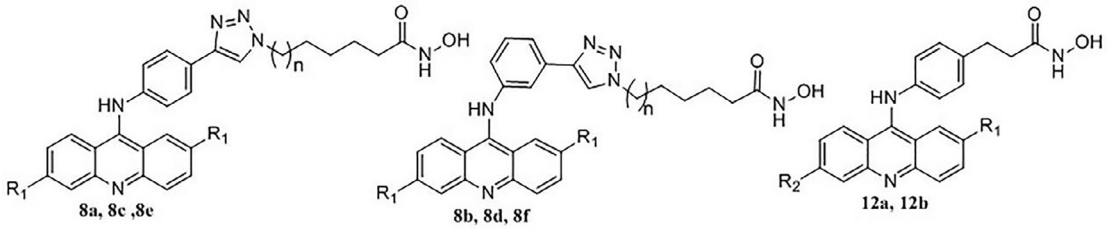

Compound	R_1	R_2	n	IC_{50} (nM)[a]	
				HDAC1	HDAC6
8a	H	H	1	8.2	2.6
8b	H	H	1	14.1	3.4
8c	H	H	2	3.9	2.9
8d	H	H	2	5.1	5.0
8e	OCH_3	Cl	1	306.2	29.0
8f	OCH_3	Cl	1	224.3	13.3
12a	H	H		133.8	99.3
12b	OCH_3	Cl		66.2	80.8
SAHA				14.3	6.9

[a] Data are expressed as mean values of at least duplicate determinations with SD values < 10% of the mean values.

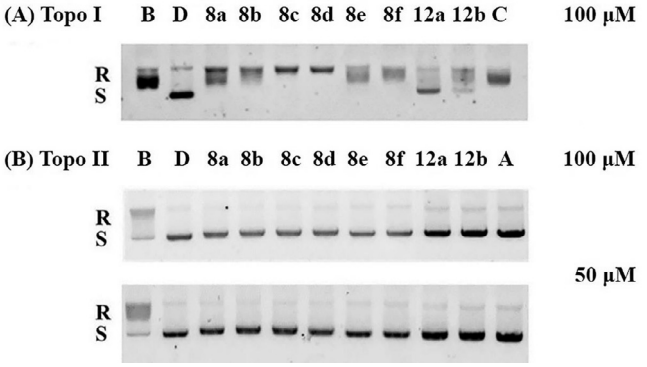

Fig. 4. Topo I and Topo II inhibitory activities. (A) Topo I: lane B, Topo I + pBR322 DNA; lane D, pBR322 DNA; lane C, camptothecin + Topo I + pBR322DNA; the others, tested compounds + Topo I + pBR322 DNA; R, relaxed; S, supercoiled. (B) Topo II: lane B, Topo II + pBR322 DNA; lane D, pBR322 DNA; lane A, *m*-AMSA + Topo II + pBR322 DNA; the others, tested compounds + Topo II + pBR322 DNA; R, relaxed; S, supercoiled.

4. Experimental section

4.1. Chemistry

The general preparation of compound (**3a–3d**, **6a–6b**, **11a–11b**) can be seen in Supporting Information.

4.1.1. General procedure for compound 8a–8f

A mixture of **3** (1.0 equiv), **6** (2.0 equiv), $CuSO_4{\cdot}5H_2O$ (0.1 equiv), sodium ascorbate (1.0 equiv) were stirred in water/TBA (v/v = 1/1) for 4 h at 60 °C under nitrogen atmosphere. Then the mixture was poured into water to give viscous solid. The viscous solid was dissolved in TEA and extracted with DCM. The organic layer was purified by column chromatography using petroleum ethyl acetate, methanol and TEA (40:1:1 v/v/v) to give pure **7a–7f**. A few drops of hydrochloric acid (3M) were added dropwise to the methanol solution of **7**. The reaction mixture was stirred at room temperature for 2 h. Concentration in vacuo gave crude product. Then the crude product was dissolved in water/methanol and extracted with DCM. The water layer was concentrated in vacuo to give solid **8a–8f**.

*4.1.1.1. 6-(4-(4-(Acridin-9-ylamino)phenyl)-1H-1,2,3-triazol-1-yl)-N-hydroxyhexanamide (**8a**).* Yield 48%; mp: 247–249 °C; ^{1}H NMR (400 MHz, DMSO-d_6) δ 10.38 (s, 1H), 8.68 (s, 2H), 8.29 (d, J = 8.6 Hz, 2H), 8.08 (s, 1H), 8.06 (s, 1H), 8.02–7.94 (m, 4H), 7.52–7.42 (m, 4H), 4.42 (t, J = 6.9 Hz, 2H), 1.96 (t, J = 7.3 Hz, 2H), 1.92–1.84 (m, 2H), 1.59–1.51 (m, 2H), 1.29–1.22 (m, 2H). ^{13}C NMR (101 MHz, DMSO-d_6) δ 168.83, 154.74, 145.48, 140.12, 135.06, 126.34, 125.73, 124.45, 123.64, 121.46, 119.18, 114.07, 49.38, 31.95, 29.95, 25.36, 24.39. HRMS (ESI): *m/z* calcd for C27H27N6O2 ($M+H^+$): 467.2195, found: 467.2196.

*4.1.1.2. 6-(4-(3-(Acridin-9-ylamino)phenyl)-1H-1,2,3-triazol-1-yl)-N-hydroxyhexanamide (**8b**).* Yield 48%; mp: 180–182 °C; ^{1}H NMR (400 MHz, DMSO-d_6) δ 10.36 (s, 1H), 8.68 (s, 1H), 8.63 (s, 1H), 8.25 (s, 2H), 8.10–7.91 (m, 4H), 7.86 (d, J = 17.8 Hz, 2H), 7.56 (s, 1H), 7.41 (s, 2H), 7.30 (s, 1H), 4.38 (s, 2H), 2.11–1.71 (m, 4H), 1.63–1.42 (m, 2H), 1.34–1.12 (m, 2H). ^{13}C NMR (101 MHz, CD3OD) δ 170.65, 145.71, 142.23, 140.58, 134.27, 132.03, 129.92, 124.89, 123.25, 122.48, 120.85, 119.70, 118.90, 114.19, 49.32, 31.45, 28.86, 24.89, 23.99. HRMS (ESI): *m/z* calcd for C27H27N6O2 ($M+H^+$): 467.2195, found: 467.2192.

*4.1.1.3. 7-(4-(4-(Acridin-9-ylamino)phenyl)-1H-1,2,3-triazol-1-yl)-N-hydroxyheptanamide (**8c**).* Yield 48%; mp: 210–212 °C; ^{1}H NMR (400 MHz, DMSO-d_6) δ 10.37 (s, 1H), 8.69 (s, 2H), 8.31 (d, J = 8.7 Hz, 2H), 8.11 (s, 1H), 8.09 (s, 1H), 8.04–7.96 (m, 4H), 7.54–7.45 (m, 4H), 4.41 (t, J = 6.9 Hz, 2H), 1.95 (t, J = 7.3 Hz, 2H), 1.91–1.84 (m, 2H), 1.53–1.46 (m, 2H), 1.32–1.26 (m, 4H). ^{13}C NMR (100 MHz, DMSO-d_6) δ 168.94, 154.96, 145.44, 140.06, 135.22, 126.34, 125.69, 124.72, 123.78, 121.50, 119.21, 113.89, 49.47, 32.07, 29.40, 27.88, 25.49, 24.82. HRMS (ESI): *m/z* calcd for C28H29N6O2 ($M+H^+$): 481.2352, found: 481.2341.

4.1.1.4. 7-(4-(3-(Acridin-9-ylamino)phenyl)-1H-1,2,3-triazol-1-yl)-N-

Table 2
Inhibitory activities of compounds against U937 cells.

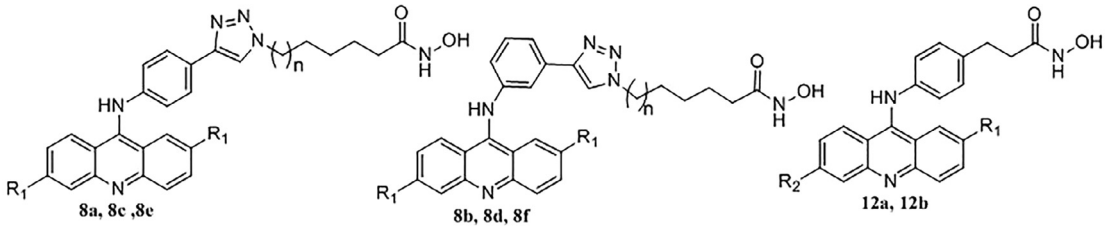

Compound	R_1	R_2	n	IC_{50} (μM)[a]
8a	H	H	1	1.34 ± 0.02
8b	H	H	1	2.67 ± 0.21
8c	H	H	2	0.90 ± 0.01
8d	H	H	2	1.24 ± 0.12
8e	OCH_3	Cl	1	3.55 ± 0.09
8f	OCH_3	Cl	1	2.94 ± 0.12
12a	H	H		0.75 ± 0.13
12b	OCH_3	Cl		1.12 ± 0.06
***m*-AMSA**				0.61 ± 0.03
SAHA				0.72 ± 0.17
7c				21.39 ± 1.23
11a				3.87 ± 0.14

[a] Data are expressed as the mean ± SD from the dose response curves of at least three independent experiments.

Table 3
Antiproliferative activities of compounds **8c**, **12a** against MDA-MB-231 and HCT-116 cell lines.

Compound	IC_{50} (μM)[a]	
	MDA-MB-231	HCT-116
8c	7.09 ± 0.47	2.11 ± 0.20
12a	29.08 ± 2.34	1.88 ± 0.09
***m*-AMSA**	10.05 ± 0.89	< 1
SAHA	4.93 ± 0.28	< 1

[a] Data are expressed as the mean ± SD from the dose response curves of at least three independent experiments.

*hydroxyheptanamide (**8d**)*. Yield 41%; mp: 185–187 °C; ^{1}H NMR (400 MHz, DMSO-d_6) δ 10.37 (s, 1H), 8.67 (s, 1H), 8.62 (s, 1H), 8.20 (s, 2H), 8.03–7.82 (m, 4H), 7.78 (s, 2H), 7.52 (s, 1H), 7.34 (s, 2H), 7.20 (s, 1H), 4.37 (s, 2H), 2.18 (s, 1H), 1.88 (d, *J* = 36.3 Hz, 3H), 1.46 (s, 2H), 1.25 (s, 4H). ^{13}C NMR (101 MHz, CD3OD) δ 174.26, 168.98, 153.58, 145.57, 143.84, 140.47, 134.13, 132.40, 130.33, 125.97, 122.95, 122.19, 121.59, 119.09, 115.04, 113.97, 49.45, 33.45, 32.06, 29.33, 25.45, 24.16. HRMS (ESI): *m/z* calcd for C28H29N6O2 (M + H^+): 481.2352, found: 481.2345.

*4.1.1.5. 6-(4-(4-((6-Chloro-2-methoxyacridin-9-yl)amino)phenyl)-1H-1,2,3-triazol-1-yl)-N-hydroxyhexanamide (**8e**)*. Yield 47%; mp: 265–267 °C; ^{1}H NMR (400 MHz, DMSO-d_6) δ 11.54 (s, 1H), 10.39 (s, 1H), 8.68 (s, 1H), 8.18 (s, 1H), 8.10 (t, *J* = 10.0 Hz, 2H), 7.98 (d, *J* = 8.2 Hz, 2H), 7.86 (s, 1H), 7.77 (d, *J* = 9.3 Hz, 1H), 7.52 (d, *J* = 8.3 Hz, 2H), 7.46 (d, *J* = 9.4 Hz, 1H), 4.41 (t, *J* = 6.6 Hz, 2H), 3.77 (s, 3H), 1.96 (t, *J* = 7.1 Hz, 2H), 1.92–1.83 (m, 2H), 1.60–1.50 (m, 2H), 1.31–1.22 (m, 2H). ^{13}C NMR (100 MHz, DMSO-d_6) δ168.81, 155.86, 153.16, 145.40, 140.28, 139.74, 138.87, 135.78, 129.49, 128.51, 127.87, 126.29, 124.73, 124.15, 121.51, 121.03, 117.93, 115.62, 112.06, 103.51, 55.81, 49.39, 31.94, 29.24, 25.37, 24.39. HRMS (ESI): *m/z* calcd for C28H28ClN6O3 (M + H^+): 531.1911, found: 531.1922.

*4.1.1.6. 6-(4-(3-((6-Chloro-2-methoxyacridin-9-yl)amino)phenyl)-1H-1,2,3-triazol-1-yl)-N-hydroxyhexanamide (**8f**)*. Yield 41%; mp: 189–191 °C; ^{1}H NMR (400 MHz, DMSO-d_6) δ 10.38 (s, 1H), 8.64 (s,1H), 8.19–8.18 (s, 1H) 8.13–8.09 (m, 2H), 7.96 (s, 1H), 7.86–7.81 (m, 2H,), 7.76–7.73 (m, 1H), 7.60–7.56 (m, 1H), 7.44–7.41 (m, 1H), 7.37–7.36 (m, 1H), 4.40–4.37 (t, 2H, *J* = 6.0 Hz), 3.74 (s,1H), 1.96–1.93 (m, 2H), 1.87–1.83 (m, 2H), 1.53–1.51 (m, 2H), 1.25–1.20 (m, 2H); ^{13}C NMR (101 MHz, DMSO-d_6) δ 168.81, 155.82, 153.07, 145.27, 141.61, 139.76, 138.82, 135.90, 132.52, 130.37, 128.49, 127.82, 124.16, 121.74, 121.10, 120.63, 118.00, 115.55, 112.09, 103.44, 55.75, 49.38, 33.34, 29.20, 25.32, 23.77. HRMS (ESI): *m/z* calcd for C28H28ClN6O3 (M + H^+): 531.1911, found: 531.1880.

*4.1.2. General procedure for compound **12a–12b***

Compounds **11a–11b** was dissolved in methanol/DCM (v/v = 1/1). Then hydroxylamine aqueous (10.0 equiv) and sodium methylate (5.0 equiv) were added under ice bath. After 0.5 h, the reaction mixture was moved to the room temperature for 1 h. Then the reaction solution was adjusted to pH 7–8 with HCl (1 M) to get a amount of precipitation. After filtration, the precipitation was washed with ether overnight to obtain pure product **12a–12b**.

*4.1.2.1. 3-(4-(Acridin-9-ylamino)phenyl)-N-hydroxypropanamide (**12a**)*. Yield 48%; mp: 195–197 °C; ^{1}H NMR (400 MHz, DMSO-d_6) δ 10.44 (s, 1H), 8.77 (s, 1H), 8.03 (s, 2H), 7.76 (s, 4H), 7.23 (s, 4H), 7.04 (s, 2H), 2.92–2.79 (m, 2H), 2.39–2.20 (m, 2H). ^{13}C NMR (101 MHz, DMSO-d_6) δ 168.08, 152.29, 140.91, 133.04, 129.46, 126.13, 122.15, 121.15, 119.07, 115.84, 33.95, 30.33. HRMS (ESI): *m/z* calcd for C22H20N3O2 (M + H^+): 358.1556, found: 358.1564.

*4.1.2.2. 3-(4-((6-Chloro-2-methoxyacridin-9-yl)amino)phenyl)-N-hydroxypropanamide (**12b**)*. Yield 48%; mp: 205–207 °C; ^{1}H NMR (400 MHz, DMSO-d_6) δ 10.39 (s, 1H), 9.11 (s, 1H), 8.75 (s, 1H), 8.12–7.95 (m, 2H), 7.53–7.35 (m, 2H), 7.29–7.02 (m, 3H), 6.77 (s, 2H), 3.74 (s, 3H), 2.85–2.67 (m, 2H), 2.35–2.11 (m, 2H). ^{13}C NMR (101 MHz, DMSO-d_6) δ 168.19, 155.70, 147.78, 146.91, 143.24, 133.50, 133.41, 131.07, 128.77, 127.56, 126.37, 125.09, 124.57,

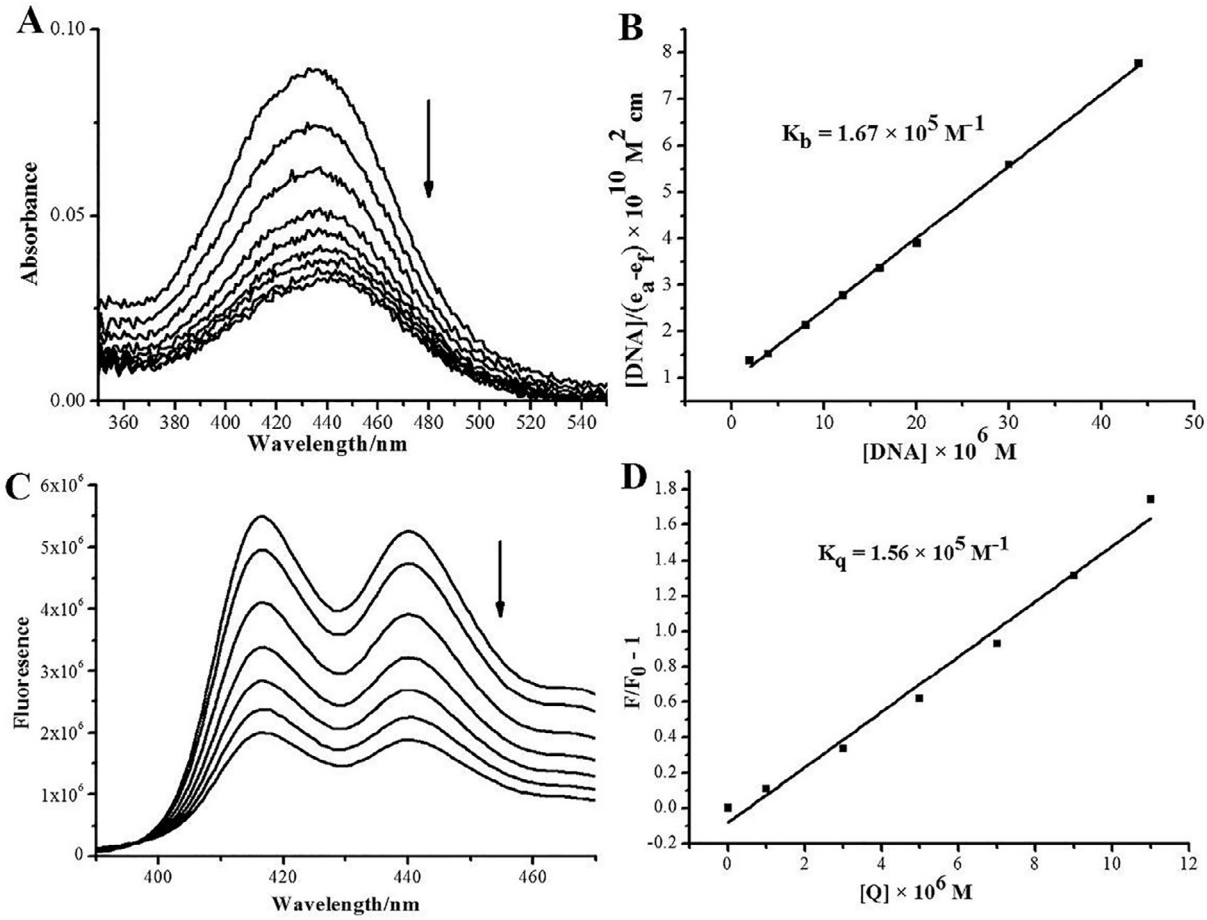

Fig. 5. UV–visible absorption spectra and fluorescence emission spectra of **8c**-ctDNA. (A) UV–visible absorption spectra **8c** (10 μM) with various concentrations of ctDNA in Tris-HCl buffer (pH 7.4). The arrow indicates the absorbance changes upon increasing DNA concentrations. (B) The plot of absorption data, [DNA], DNA concentration. (C) Fluorescence emission spectra of **8c** (10 μM) with various concentrations of ctDNA in Tris-HCl buffer (pH 7.4) after excitation at λ_{ex} = 360 nm. The arrow indicates the fluorescence emission changes upon increasing DNA concentrations. (D) The plots of the fluorescence titration, [Q], DNA concentration.

120.34, 118.08, 117.62, 100.66, 55.22, 34.01, 30.13. HRMS (ESI): *m/z* calcd for C23H21ClN3O3 ($M+H^+$): 422.1271, found: 422.1252.

4.2. Cell proliferation inhibitory assays

Cell proliferation inhibitory assays were assessed by the MTT assay. Cells were seeded in 96-well plates at a density of 5–10 × 10^3 cells per well with incubation for 12 h at 37 °C. Then various concentrations of the synthesized compounds or blank control DMSO were added to each well and incubated continuously for 48 h. After adding 10 mL per well of MTT (5 mg/mL) solution for 4 h, the formazan crystals were dissolved in 100 mL DMSO per well. The absorbance of each well was measured at 490 nm using an automatic ELISA reader system (TECAN, CHE).

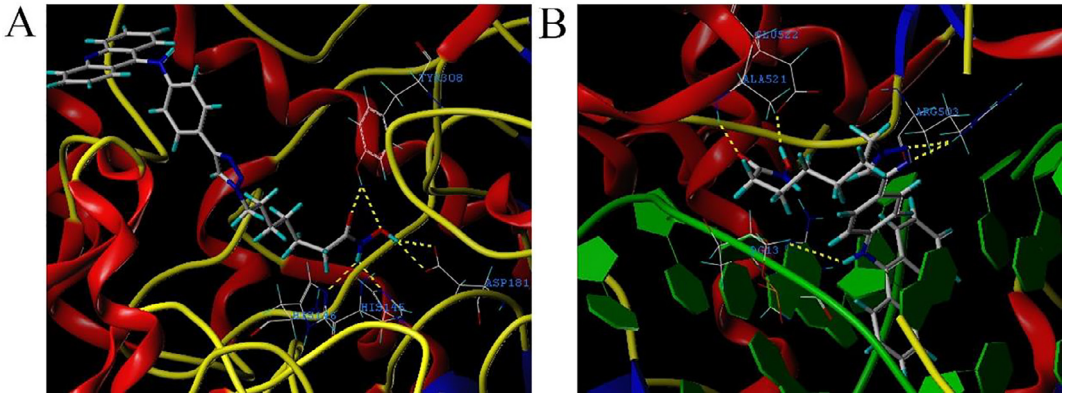

Fig. 6. Molecular docking of compounds **8c** with HDAC2 and Topo II-DNA complex. (A) Proposed binding mode of compounds **8c** with HDAC2 (4LXZ), (B) Proposed binding mode of compounds **8c** with Topo II (4G0U) (N and O atoms in blue and red, respectively). (For interpretation of the references to colour in this figure legend, the reader is referred to the web version of this article.)

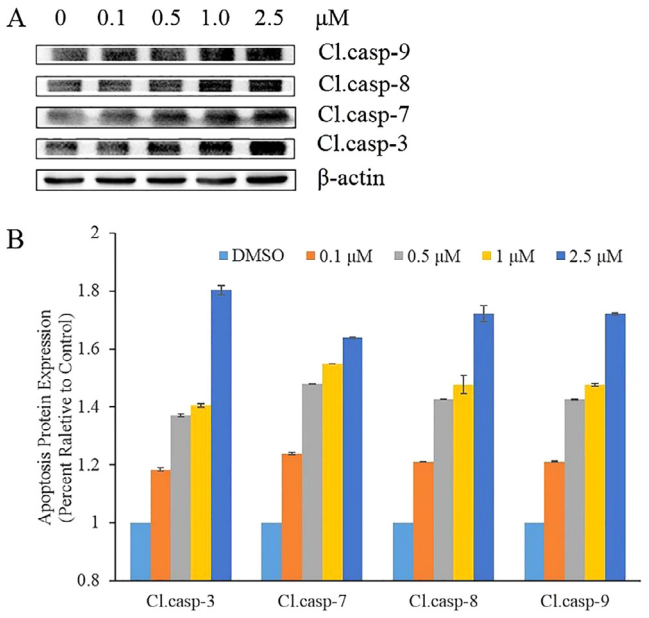

Fig. 7. Western blot analysis of U937 cells treated with compound **8c** at indicated concentrations for 36 h.

4.3. HDAC inhibition assay

The procedures of HDAC inhibition assay were as follows: the synthesized compounds were transferred to assay plate by echo with 3-fold dilution in 100% DMSO. Substrate solution was produced by preparing enzyme solution in 1× assay buffer (modified Tris Buffer) and adding trypsin and Ac-peptide substrate in 1× assay buffer. Enzyme solution were transferred to assay plate and incubated at room temperature for 15 min. Substrate solution was then added to each well to start reaction. SAHA was used as the positive controls and the negative controls contained neither enzyme nor inhibitor. The plates were incubated for 1 h at room temperature to allow the fluorescence signal to develop. The fluorescence generated was monitored at λ_{ex} = 355 nm and λ_{em} = 460 nm using a Synergy MX plate reader (PerkinElmer Life Sciences, Boston, MA, USA).

4.4. Topo I and Topo II inhibition assay

The way to define the Topo I and Topo II inhibition of the synthesized compounds was to dissect the relaxation of supercoiled pBR322 plasmid DNA. The assay was carried out in a final volume of 20 μL reaction volume containing 500 ng of supercoiled DNA (Takara Biotechnology, Japan) and 1 unit of human Topo I (Takara Biotechnology, Japan) or Topo II (USB Corp, USA) with our compounds or reference compounds in the reaction buffer. The reaction mixtures were incubated at 37 °C for 10–15 min and terminated by adding 4 μL of DNA loading buffer. Electrophoresis was performed on a 1% agarose gel at 80 V for 0.5 h in TAE buffer. Then gels were stained for 10 min with ethidium bromide (2.5 mg/mL) and destained in water for 5 min. DNA bands were visualized with UV light. Topo I inhibitor camptothecin (Sigma, USA) and Topo II inhibitor *m*-AMSA (Sigma, USA) were used as reference compounds.

4.5. Western blot analysis

U937 cells were treated with compound **8c** at the concentrations of 0 μM, 0.1 μM, 0.5 μM, 1 μM and 2.5 μM for 36 h. Then U937 cells were harvested and handled with lysis buffer at 0 °C for 0.5 h, followed by centrifugation at 13,000*g* for 10 min. The supernatants were heated with loading buffer to 100 °C for 10 min after their protein concentrations were determined with BCA Protein Assay Kit (Tiangen). Protein samples were subjected to 12% sodium dodecylsulfate (SDS)–polyacrylamide gel electrophoresis (PAGE), and then transferred to menthol treated PVDF membranes (amc Biobind NT-200). The membranes should be blocked in 5% milk for 1 h before they were incubated with certain primary antibody at 4 °C overnight. The primary antibody dilution was 1:1000. The membrane was finally incubated with a HRP-conjugated anti-mouse or anti-rabbit second antibodies for 2 h before it was visualized with BeyoECL Plus (Beyotime) using the BIO-RAD Gel Doc XR. Each time when the incubation solutions were switched, the membranes should be washed with TBST for 3 × 5 min.

4.6. Molecular docking

The molecular modeling of compounds were performed with the molecular modeling package SYBYL-X 1.3 (Tripos associate Inc., St. Louis, MO, USA). Three dimensional structures of HDAC2 (PDB code: 4LXZ) and Topo II-DNA complex (PDB code: 4G0U) were downloaded from Protein Data Bank (PDB). Hydrogen atoms were added. The general procedure is as followed: (a) ligands and enzymes preparation; (b) protocol generation; (c) docking and scoring; and (d) results analyzing.

Acknowledgements

We appreciate the financial supports from Shenzhen Municipal government SZSITIC (JCYJ20160301153753269) and China Postdoctoral Science Foundation (Grant Number: 2018M631825).

A. Supplementary data

Supplementary data (the ^{1}H-NMR, ^{13}C NMR and high resolution mass spectrometry of synthesized compounds) associated with this article can be found, in the online version, at http://dx.doi.org/10.1016/j.bmc.2018.06.016.

References

1. Morphy R, Rankovic Z. Designed multiple ligands. An emerging drug discovery paradigm. *J Med Chem.* 2005;48:6523–6543.
2. Morphy R, Kay C, Rankovic Z. From magic bullets to designed multiple ligands. *Drug Discov Today.* 2004;9:641–651.
3. Falkenberg KJ, Johnstone RW. Histone deacetylases and their inhibitors in cancer, neurological diseases and immune disorders. *Nat Rev Drug Discov.* 2014;13:673–691.
4. Roche J, Bertrand P. Inside HDACs with more selective HDAC inhibitors. *Eur J Med Chem.* 2016;121:451–483.
5. Raji I, Yadudu F, Janeira E, et al. Bifunctional conjugates with potent inhibitory activity towards cyclooxygenase and histone deacetylase. *Bioorg Med Chem.* 2017;25:1202–1218.
6. Yao L, Mustafa N, Tan EC, et al. Design and synthesis of ligand efficient dual inhibitors of janus kinase (JAK) and histone deacetylase (HDAC) based on ruxolitinib and vorinostat. *J Med Chem.* 2017;60:8336–8357.
7. Peng FW, Xuan J, Wu TT, et al. Design, synthesis and biological evaluation of *n*-phenylquinazolin-4-amine hybrids as dual inhibitors of VEGFR-2 and HDAC. *Eur J Med Chem.* 2016;109:1–12.
8. Liu J, Qian C, Zhu Y, et al. Design, synthesis and evaluate of novel dual FGFR1 and HDAC inhibitors bearing an indazole scaffold. *Bioorg Med Chem.* 2018;26:747–757.
9. Cuadrado-Tejedor M, Garcia-Barroso C, Sanchez-Arias JA, et al. A first-in-class small-molecule that acts as a dual inhibitor of HDAC and PDE5 and that rescues hippocampal synaptic impairment in alzheimer's disease mice. *Neuropsychopharmacol.* 2017;42:524–539.
10. Amemiya S, Yamaguchi T, Hashimoto Y, et al. Synthesis and evaluation of novel dual BRD4/HDAC inhibitors. *Bioorg Med Chem.* 2017;25:3677–3684.
11. Kalin JH, Wu M, Gomez AV, et al. Targeting the corest complex with dual histone deacetylase and demethylase inhibitors. *Nat Commun.* 2018;9:53.
12. Pommier Y. Drugging topoisomerases: lessons and challenges. *ACS Chem Biol.* 2013;8:82–95.
13. Pommier Y, Sun Y, Huang SN, et al. Roles of eukaryotic topoisomerases in transcription, replication and genomic stability. *Nat Rev Mol Cell Biol.* 2016;17:703–721.
14. Zhang B, Li X, Li B, et al. Acridine and its derivatives: a patent review (2009–2013). *Expert Opin Ther Pat.* 2014;24:647–664.
15. Yuan Z, Chen S, Chen C, et al. Design, synthesis and biological evaluation of 4-amidobenzimidazole acridine derivatives as dual PARP and Topo inhibitors for cancer therapy. *Eur J Med Chem.* 2017;138:1135–1146.
16. Cui Z, Li X, Li L, et al. Design, synthesis and evaluation of acridine derivatives as multi-target Src and MEK kinase inhibitors for anti-tumor treatment. *Bioorg Med*

Chem. 2016;24:261–269.
17. Luan X, Gao C, Zhang N, et al. Exploration of acridine scaffold as a potentially interesting scaffold for discovering novel multi-target VEGFR-2 and Src kinase inhibitors. *Bioorg Med Chem.* 2011;19:3312–3319.
18. Zhang W, Zhang B, Zhang W, et al. Synthesis and antiproliferative activity of 9-benzylamino-6-chloro-2-methoxy-acridine derivatives as potent DNA-binding ligands and topoisomerase II inhibitors. *Eur J Med Chem.* 2016;116:59–70.
19. Gao C, Li B, Zhang B, et al. Synthesis and biological evaluation of benzimidazole acridine derivatives as potential DNA-binding and apoptosis-inducing agents. *Bioorg Med Chem.* 2015;23:1800–1807.
20. Li D, Yuan Z, Chen S, et al. Synthesis and biological research of novel azaacridine derivatives as potent DNA-binding ligands and topoisomerase II inhibitors. *Bioorg Med Chem.* 2017;25:3437–3446.
21. Catalano MG, Fortunati N, Pugliese M, et al. Valproic acid, a histone deacetylase inhibitor, enhances sensitivity to doxorubicin in anaplastic thyroid cancer cells. *J Endocrinol.* 2006;191:465–472.
22. Kim MS, Blake M, Baek JH, et al. Inhibition of histone deacetylase increases cytotoxicity to anticancer drugs targeting DNA. *Cancer Res.* 2003;63:7291–7300.
23. Marchion DC, Bicaku E, Turner JG, et al. Synergistic interaction between histone deacetylase and topoisomerase II inhibitors is mediated through topoisomerase IIbeta. *Clin Cancer Res.* 2005;11:8467–8475.
24. Bruzzese F, Rocco M, Castelli S, et al. Synergistic antitumor effect between vorinostat and topotecan in small cell lung cancer cells is mediated by generation of reactive oxygen species and DNA damage-induced apoptosis. *Mol Cancer Ther.* 2009;8:3075–3087.
25. Gray J, Cubitt CL, Zhang S, et al. Combination of HDAC and topoisomerase inhibitors in small cell lung cancer. *Cancer Biol Ther.* 2014;13:614–622.
26. Johnson CA, Padget K, Austin CA, et al. Deacetylase activity associates with topoisomerase II and is necessary for etoposide-induced apoptosis. *J Biol Chem.* 2001;276:4539–4542.
27. Marchion DC, Bicaku E, Daud AI, et al. Sequence-specific potentiation of topoisomerase II inhibitors by the histone deacetylase inhibitor suberoylanilide hydroxamic acid. *J Cell Biochem.* 2004;92:223–237.
28. Munster PN, Marchion DC, Bicaku E, et al. Phase I trial of a sequence-specific combination of the HDAC inhibitor, valproic acid (VPA), and the topoisomerase II inhibitor, epirubicin, in advanced solid tumors: clinical results and correlative studies. *J Clin Oncol.* 2006;24 3068–3068.
29. Na YS, Kim SM, Jung KA, et al. Effects of the HDAC inhibitor CG2 in combination with irinotecan, 5-fluorouracil, or oxaliplatin on HCT116 colon cancer cells and xenografts. *Oncol Rep.* 2010;24:1509–1514.
30. Ocker M, Alajati A, Ganslmayer M, et al. The histone-deacetylase inhibitor SAHA potentiates proapoptotic effects of 5-fluorouracil and irinotecan in hepatoma cells. *J Cancer Res Clin Oncol.* 2005;131:385–394.
31. Sarcar B, Kahali S, Chinnaiyan P. Vorinostat enhances the cytotoxic effects of the topoisomerase I inhibitor SN38 in glioblastoma cell lines. *J Neurooncol.* 2010;99:201–207.
32. Sato A, Asano T, Horiguchi A, et al. Antitumor effect of suberoylanilide hydroxamic acid and topotecan in renal cancer cells. *Oncol Res.* 2011;19:217–223.
33. Cincinelli R, Musso L, Artali R, et al. Camptothecin-psammaplin a hybrids as topoisomerase I and HDAC dual-action inhibitors. *Eur J Med Chem.* 2018;143:2005–2014.
34. Guerrant W, Patil V, Canzoneri JC, et al. Dual targeting of histone deacetylase and topoisomerase II with novel bifunctional inhibitors. *J Med Chem.* 2012;55:1465–1477.
35. Guerrant W, Patil V, Canzoneri JC, et al. Dual-acting histone deacetylase-topoisomerase I inhibitors. *Bioorg Med Chem Lett.* 2013;23:3283–3287.
36. He S, Dong G, Wang Z, et al. Discovery of novel multiacting topoisomerase I/II and histone deacetylase inhibitors. *ACS Med Chem Lett.* 2015;6:239–243.
37. Seo YH. Dual inhibitors against topoisomerases and histone deacetylases. *J Cancer Prev.* 2015;20:85–91.
38. Yamashita M, Tahara T, Hayakawa S, et al. Synthesis and biological evaluation of histone deacetylase and DNA topoisomerase II-targeted inhibitors. *Bioorg Med Chem.* 2018.
39. Yu CC, Pan SL, Chao SW, et al. A novel small molecule hybrid of vorinostat and DACA displays anticancer activity against human hormone-refractory metastatic prostate cancer through dual inhibition of histone deacetylase and topoisomerase I. *Biochem Pharmacol.* 2014;90:320–330.
40. Zhang X, Bao B, Yu X, et al. The discovery and optimization of novel dual inhibitors of topoisomerase II and histone deacetylase. *Bioorg Med Chem.* 2013;21:6981–6995.
41. Lang X, Li L, Chen Y, et al. Novel synthetic acridine derivatives as potent DNA-binding and apoptosis-inducing antitumor agents. *Bioorg Med Chem.* 2013;21:4170–4177.
42. Hou J, Feng C, Li Z, et al. Structure-based optimization of click-based histone deacetylase inhibitors. *Eur J Med Chem.* 2011;46:3190–3200.
43. Chowdhury I, Tharakan B, Bhat GK. Caspases - an update. *Comp Biochem Physiol B: Biochem Mol Biol.* 2008;151:10–27.